

# Self-Healable Poly(Acrylic Acid) Binder toward Optimized Electrochemical Performance for Silicon Anodes: Importance of Balanced Properties

Anjali Nagapadi Preman, Thuan Ngoc Vo, Subi Choi, Hyocheol Lee, Ye Eun Lim, Il Tae Kim,\* and Suk-kyun Ahn\*



Cite This: *ACS Appl. Energy Mater.* 2024, 7, 749–759



Read Online

ACCESS |



Metrics & More



Article Recommendations

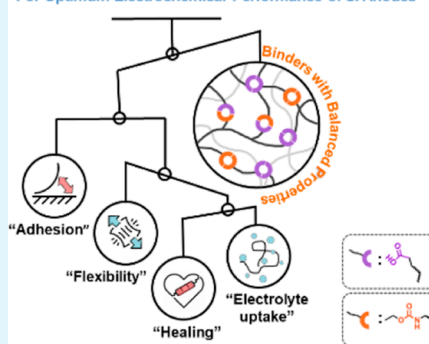


Supporting Information

**ABSTRACT:** Si is a promising anode for high-energy lithium-ion batteries, but its severe capacity decay due to volume changes remains a challenge. To address this, we synthesized a series of acrylic copolymer binders with randomly distributed carboxylic acid (CA) and *n*-butyl carbamate (BC) groups. CA groups ensure good adhesion to the Si surface, while BC groups provide self-healing as well as a wide range of thermal and mechanical properties. By fine-tuning the content of these functional groups, we optimize the mechanical, adhesion, and self-healing properties, and electrolyte uptake of the binders to maximize their electrochemical performance. The Si electrode with a binder containing 68 mol % CA groups and 32 mol % BC groups achieves a high initial discharge capacity of 3628 mA h g<sup>-1</sup>, with an initial Coulombic efficiency (ICE) of 84%. This electrode also displays a discharge capacity of 2334 mA h g<sup>-1</sup> after 100 cycles at 0.5 A g<sup>-1</sup>, surpassing the performance of a Si-poly(acrylic acid) electrode (3171 mA h g<sup>-1</sup> at the first cycle, ICE of 86%, and 1367 mA h g<sup>-1</sup> at the 100th cycle at 0.5 A g<sup>-1</sup>). Through a systematic investigation of the structure–property–electrochemical performance relationship, we prioritize the desired properties of the binder to enable the development of high-performance Si anodes.

**KEYWORDS:** self-healing, binder, Si anode, lithium-ion batteries, copolymers

For Optimum Electrochemical Performance of Si Anodes



## INTRODUCTION

Lithium-ion batteries (LIBs) are some of the most efficient and economical energy storage systems suitable for use in the modern era.<sup>1</sup> Although state-of-the-art LIBs are substantially advanced in various respects, including a 4-fold increase in energy density, significantly reduced recharging time, and enhanced safety, the energy density of the conventional electrodes (graphite/LiMO<sub>x</sub>) is close to saturation, necessitating the development and use of high-energy alternatives.<sup>2–4</sup> To this end, Si attracts significant attention, owing to its excellent electrochemical features. Unlike graphite anodes that may store only 1/6 Li ions per atom, each Si may host up to 4.4 Li ions, forming lithium silicates with 10-fold higher capacities (4200 mA h g<sup>-1</sup> for Li<sub>4.4</sub>Si and 372 mA h g<sup>-1</sup> for LiC<sub>6</sub>).<sup>5</sup> Moreover, its earth abundance, innocuous nature, and mature processing techniques render it viable for use in next-generation LIB anodes.<sup>6,7</sup>

In practice, however, Si is not utilized as the major anode component in commercial LIBs owing to the low capacity retention caused by considerable volume expansion/shrinkage during lithiation/delithiation. In Si anodes, capacity decay is predominantly caused by the continuous growth of the solid electrolyte interphase (SEI) and mechanical deterioration of the electrode in the form of particle pulverization and

delamination from the metallic current collector.<sup>8</sup> Various nano, porous, and hybrid electrode structures have been explored to overcome the critical problems of the Si anode.<sup>9–13</sup> These elegantly engineered structures exhibit enhanced structural integrity and resistance to mechanical breakdown; however, their practical application is hampered by low areal mass loadings, in addition to demanding, complicated processing.<sup>14</sup>

The use of a rationally designed polymer binder is an alternative strategy to address the drastic consequences of volume expansion.<sup>15</sup> Although the binder is electrochemically inert and constitutes only a small proportion of the electrode, its properties are critical for ensuring the uniform dispersion of active materials and a conductive agent in the slurry and their adhesion to the metallic current collector as well as effective stress dissipation.<sup>16</sup> Although polyvinylidene fluoride and carboxymethyl cellulose (CMC)/styrene–butadiene rubber

**Received:** November 9, 2023

**Revised:** December 14, 2023

**Accepted:** December 19, 2023

**Published:** December 29, 2023



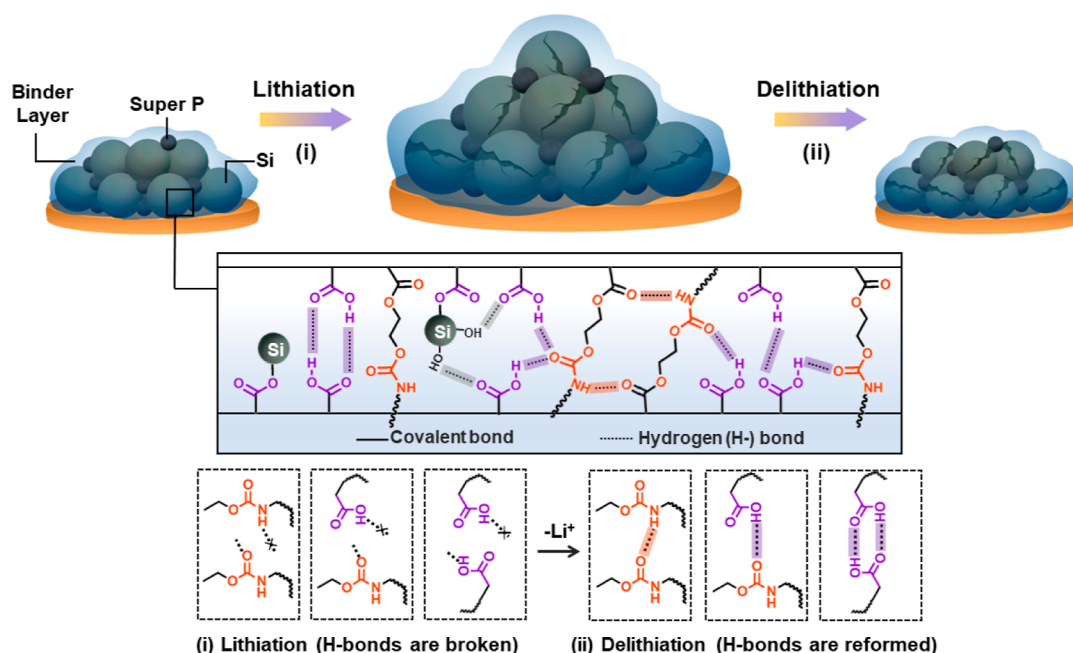


**Figure 1.** Functions of the newly designed copolymer binder: covalent bonds and various types of hydrogen bonds, along with mechanical toughness, may result in strong interactions with the Si surface and conductive agents that aid in preserving the structural integrity of the Si anode during (i) lithiation and (ii) delithiation.

are widely used in commercial LIBs, their application in Si-based systems is ineffective due to their incompatibilities with the hydrophilic surface features of Si and inadequate mechanical strength.<sup>17</sup> According to previous studies, polymers with polar functional groups (e.g.,  $-\text{OH}$ ,  $-\text{NH}_2$ , and  $-\text{COOH}$ ) display improved adhesion to the Si surface. Various natural polysaccharides, including CMC,<sup>18,19</sup> alginate,<sup>20</sup> and chitosan,<sup>8</sup> have received considerable attention in this regard.

In 2010, Yushin group first introduced poly(acrylic acid) (PAA), which may strongly adhere to the Si surface via multiple physical and chemical bonds formed by its abundant carboxylic acid groups, for use in Si anodes.<sup>21</sup> However, simply enhancing the adhesion strength of the binder does not seem sufficient to circumvent undesirable volume expansion. In addition to adhesion, viscoelastic properties and mechanical robustness are critical for accommodating immense stress and maintaining the integrity of an electrode during volume changes. Incorporation of a soft moiety or fabrication of network structures is effective in modulating the mechanical properties of PAA and thus stabilizing the electrode.<sup>22–26</sup> Remarkably, Choi et al. developed a topology-controlled binder by covalently integrating a pulley cross-linker, polyrotaxane (PR), into linear PAA. High elasticity due to the mobile rings of PR aids in accommodating the large strain caused by the expansion of a micro-Si anode.<sup>27</sup>

Recently, self-healing binders received increasing attention in the fabrication of Si anodes because of their capacities to repair structural damage, which may significantly benefit the preservation of electrode integrity and electronic contact.<sup>4,23,28–33</sup> For example, Bao and co-workers utilized a stretchable polymer comprising urea groups that offer abundant hydrogen bonding, thereby providing self-healing properties to enhance the stabilities of Si anodes.<sup>34</sup> Zhang et al. designed a supramolecular binder comprising AA and ureidopyrimidinone (UPy) in which the UPy moiety can strongly bind with active materials and provide a self-healing

property via quadruple hydrogen bonding, resulting in Si anodes with enhanced electrochemical performance.<sup>35</sup> Jeon and co-workers demonstrated the recovery of manually induced damage in electrodes via the dynamic hydrogen bonding and electrostatic attraction of a ternary hybrid binder comprising poly(3,4-ethylenedioxythiophene), PAA, and phytic acid.<sup>36</sup> Although several reports claim that self-healing is critical to stable cycling, whether a self-healing binder is the most essential for determining the quality and lifetime of Si anodes remains unclear. Over the decades, numerous studies independently investigated various types of binders in terms of adhesion, electrolyte uptake, elasticity, and self-healing properties.<sup>21,34,37–41</sup> However, systematic studies regarding the structure–property–electrochemical performance relationship, involving a series of binders containing multiple functionalities, have not been extensively conducted.

To determine the key parameters of the binder that favor the electrochemical performance of an Si anode, herein, we synthesized a series of novel random copolymers, namely, AA(xx)UR(yy), comprising various contents of carboxylic acid and *n*-butyl carbamate moieties. The carboxylic acid groups strongly adhered to the Si surface, whereas *n*-butyl carbamate was introduced to allow compliance via its flexible alkyl side chains in addition to self-healing via various types of hydrogen bonding interactions. Saito and co-workers, in particular, recently reported that poly(2-[(butylamino)carbonyl]oxyethyl acrylate (BCOE)) exhibited a strong adhesion force with autonomous self-healing at room temperature owing to abundant hydrogen bonding and the flexible polymer backbone (glass transition temperature ( $T_g$ ) of  $-3\text{ }^\circ\text{C}$ ).<sup>42</sup> More recently, a copolymer prepared using the BCOE monomer was found to be an effective protective layer for an Li–metal electrode due to excellent self-healing.<sup>43</sup> Based on these results, the incorporation of the carboxylic acid (i.e., acrylic acid monomer) and *n*-butyl carbamate groups (i.e., BCOE monomer) along the polyacrylate backbone can also yield a

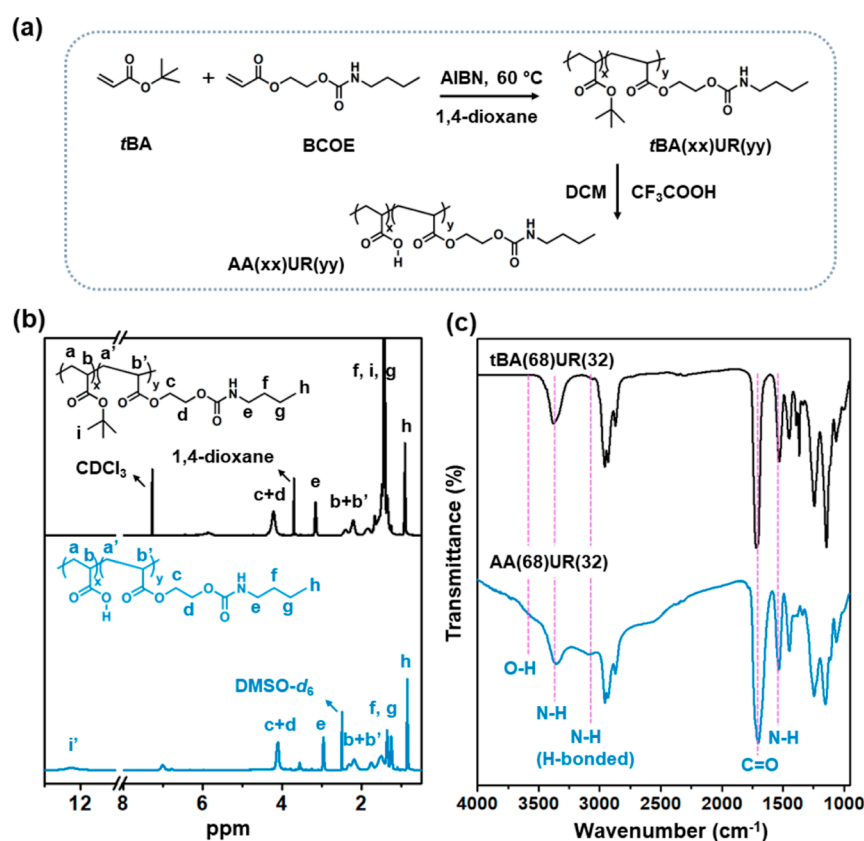


**Figure 2.** (a) Syntheses of the  $AA(xx)UR(yy)$  binders. (b)  $^1H$  NMR and (c) FT-IR spectra of the copolymers before and after removal of  $t$ -butyl protecting groups.

high-performance binder for use in the Si anode. In this study, our focus is to systematically investigate the effects of the relative functionalities of random copolymers (i.e., carboxylic acid and  $n$ -butyl carbamate groups) on the thermal, mechanical, and adhesion properties of the binders in addition to the electrochemical performance of the Si anode. To the end, we shall highlight the critical physical properties in designing an effective binder for use in the Si anode based on our system. As shown in Figure 1, the newly designed copolymer should induce strong binding with Si and conductive agents via covalent bonds and various types of dynamic hydrogen bonds. This may effectively accommodate the internal stress during lithiation and delithiation of Si, thereby preserving the mechanical integrity of the electrode. By careful adjustment of the composition of the copolymer, the adhesion, mechanical strength, and self-healing properties of the resulting binders were systematically altered, ultimately influencing the electrochemical performance of the Si anode.

## EXPERIMENTAL SECTION

**Materials.** *Tert*-Butyl acrylate ( $tBA$ , 98%, Sigma-Aldrich) and BCOE (Sigma-Aldrich) were passed through basic aluminum oxide and stored at 4 °C, and azobis(isobutyronitrile) (AIBN, 98%, Sigma-Aldrich) was recovered from acetone, recrystallized in methanol, and stored at 4 °C. 1,4-Dioxane (anhydrous, 99.8%, Sigma-Aldrich), trifluoroacetic acid (TFA, 99%, Sigma-Aldrich), dichloromethane (DCM, stabilized with ethanol, >99%, Alfa Aesar), dimethyl sulfoxide (DMSO, Sigma-Aldrich), Si nanoparticles (SiNPs, APS  $\leq 50$  nm, 98%, Alfa Aesar), and carbon black (Super P, 99+%, Alfa Aesar) were used as received.

**Synthesis of Random Copolymer Binders.**  $T$ -Butyl-protected copolymers,  $tBA(xx)UR(yy)$ , where  $xx$  and  $yy$  are the molar ratios of

$tBA$  and BCOE, were synthesized via conventional free radical polymerization. To prepare  $tBA(68)UR(32)$ ,  $tBA$  (4.48 g, 35 mmol), BCOE (3.22 g, 15 mmol), and AIBN (0.012 g, 0.07 mmol) were dissolved in anhydrous 1,4-dioxane (28 mL) and degassed for 20 min to remove trace amounts of oxygen. The mixture was polymerized for 24 h at 60 °C, and the solvent was then removed under reduced pressure. The crude product was precipitated in cold hexane and dried under a vacuum at 27 °C (6.25 g, yield 81%). For comparison, a poly( $tBA$ ) homopolymer (ptBA) was synthesized using a similar protocol.

To eliminate the  $t$ -butyl protecting group, the dried polymer,  $tBA(68)UR(32)$  (6 g, 33 mmol), was dissolved in DCM (45 mL). TFA (10.03 mL, 131 mmol) was added dropwise at room temperature under a continuous nitrogen flow to avoid side reactions. After 24 h, the mixture was concentrated under reduced pressure; the product was precipitated in cold hexane and dried under a vacuum at 27 °C to yield the deprotected polymer,  $AA(68)UR(32)$  (Figure 2a). The acrylic polymer binders (after TFA treatment) are denoted as  $AA(xx)UR(yy)$  [ $xx$  and  $yy$  indicate the mole percentages of AA and BCOE (i.e., urethane (UR)-group-functionalized monomer) monomers, respectively].

**Methods and Characterization.**  $^1H$  nuclear magnetic resonance (NMR) spectroscopy was performed by using a 500 MHz Varian spectrometer (Agilent Technologies) with  $CDCl_3$  or  $DMSO-d_6$  as the lock solvent. The molecular weights and dispersities of the synthesized polymers were determined by size exclusion chromatography (SEC), equipped with an Agilent 1100 pump, PSS SDV (5  $\mu m$ ;  $10^5$ ,  $10^3$ , and  $10^2$  Å;  $8.0 \times 300.0$  mm) columns, and a refractive index detector. To avoid clogging of the column, SEC was performed by using the protected samples,  $tBA(xx)UR(yy)$ . Tetrahydrofuran (THF) was used as the eluent at a flow rate of  $1.0 mL min^{-1}$ , and a calibration curve was constructed using poly(methyl methacrylate) (PMMA) standards. Attenuated total reflectance spectra were obtained using a Jasco FT/IR-4600 spectrometer with 32 scans



collected for each sample at a resolution of 4 cm<sup>-1</sup>. The  $T_g$  values were determined using differential scanning calorimetry (DSC, Discovery DSC 25, TA Instruments). Each sample was subjected to a heat-cool-heat cycle by heating to 150 °C, cooling to 0 °C, and reheating to 150 °C at a scan rate of 10 °C min<sup>-1</sup> in a nitrogen atmosphere. Tensile measurements were performed using a dynamic mechanical analyzer (DMA Q850, TA Instruments) and tension film clamp. The samples (length × width × thickness = 7 × 5 × 0.15 mm) were equilibrated at 25 °C under a preload of 0.001 N, and the force was increased at a rate of 0.5 N min<sup>-1</sup> until breakage. Self-healing studies were conducted at 25 °C and a relative humidity of ≤40% using a laser confocal microscope (OLSS000, Olympus). All thermal, mechanical, and electrochemical characterizations were performed by using the deprotected copolymers, AA(xx)UR(yy). The crystalline structure of Si material was characterized by X-ray diffraction (XRD, Bruker AXS) using Cu K $\alpha$  radiation ( $\lambda$  = 1.5418 Å) in the  $2\theta$  range 20–80° (Figure S1).

**Electrode Preparation and Electrochemical Characterization.** A binder solution (10 wt %) was prepared in DMSO. To prepare a slurry, the binder solution (15 wt %), super P (15 wt %), and SiNPs (70 wt %) were thoroughly mixed in a scintillation vial equipped with two magnetic stir bars for 24 h at room temperature. The resulting slurry was cast onto a battery-grade copper foil (thickness = 18  $\mu$ m) using a doctor blade and dried at 70 °C under vacuum. After drying for 24 h, the prepared electrodes were punched into circular discs ( $\varnothing$  12 mm) and paired with Li metal ( $\varnothing$  14 mm) in CR 2032-type coin cells for use in galvanostatic measurements. The density of the Si electrodes was around 300–400 mg cm<sup>-3</sup>. A polyethylene membrane ( $\varnothing$  18 mm, thickness = 12  $\mu$ m, Wellcos) and 1 M solution (200  $\mu$ L) of LiPF<sub>6</sub> in ethylene carbonate, ethyl methyl carbonate, and diethyl carbonate (v/v/v = 3/4/3, Panax Etec) with 10% fluoroethylene carbonate (FEC) were used as the separator and electrolyte, respectively. The coin cells were assembled in an argon-filled glovebox.

Galvanostatic cycling tests were performed using a battery cycler (WBCS3000L, WonATech) at 27 °C in the potential range of 0.01–1.5 V (vs Li/Li<sup>+</sup>). The prepared coin cells were aged for 12 h and cycled in constant current mode at 0.5 A g<sup>-1</sup>. The rate cyclability of the cells was evaluated by varying the current density from 0.2 to 2.0 A g<sup>-1</sup>. Additionally, selected cells were cycled at high current densities of 4.0 and 8.0 A g<sup>-1</sup>. Electrochemical impedance spectroscopy (EIS) was conducted using a ZIVE MP1 station (WonATech) at 1.5 V over frequencies ranging from 100 kHz to 100 mHz. A ZMAN version 2.4 simulator (WonATech) was employed to regress various impedance parameters.

**Adhesion Test.** The adhesion properties of the electrodes were evaluated using a universal testing machine (UTM, Dr TECH, DR-100) and at least three rectangular sections of each electrode. 3 M tape (width = 18 mm) attached to the laminated side of the electrode was pulled at an angle of 180° at a constant displacement rate of 40 mm min<sup>-1</sup>, and the force required to peel off the laminate from the surface of the current collector was recorded.

**Post-mortem Analyses of Cycled Electrodes.** For post-mortem analysis, the coin cells were disassembled in the argon-filled glovebox. The cycled electrodes were carefully separated, rinsed with dimethyl carbonate, and dried inside the glovebox. Surface and cross-sectional images of the electrodes were obtained through scanning electron microscopy (SEM, Supra 25, ZEISS); for this analysis, each electrode was coated with a layer of platinum (thickness = 8 nm) to eliminate charge. For cross-sectional imaging, the electrode was immersed in liquid nitrogen and manually fractured while frozen.

**Electrolyte Uptake.** To measure electrolyte uptake, rectangular films of each binder (thickness  $\approx$  150  $\mu$ m) were immersed in the electrolyte at room temperature for 24 h. The masses of the swollen films were measured after the residual solvent was wiped from their surfaces. The binders containing >32 mol % of urethane groups displayed excessive swelling and stuck to the surfaces of the glass vials; thus, their measurements were excluded. The electrolyte uptake is determined using the following equation

$$\text{electrolyte uptake(\%)} = \frac{W_s - W_i}{W_i} \times 100$$

where  $W_i$  and  $W_s$  are the masses of the original dried and electrolyte-swollen films, respectively.

## RESULTS AND DISCUSSION

**Synthesis and Characterization of Copolymer Binders.** We synthesized a series of random copolymer binders comprising carboxylic acid and *n*-butyl carbamate moieties. The carboxylic acid groups were introduced to induce a high affinity for the Si surface, whereas the *n*-butyl carbamate groups were employed to exploit their strong hydrogen bonding capabilities via intra- or intermolecular interactions. The acrylic random copolymers are synthesized in two steps: first, by simultaneously copolymerizing *t*BA and BCOE via free radical polymerization using AIBN, followed by cleavage of the *t*-butyl groups using TFA (Figure 2a). The copolymers containing various contents of carboxylic acid and *n*-butyl carbamate functionalities with comparable molecular weights were successfully synthesized. The molecular weights and molecular weight distributions of the copolymers were analyzed through SEC. Notably, the molecular weights of all synthesized polymers, including *pt*BA, are  $\sim$ 100 kDa, with dispersities of <2.0 (Figure S2 and Table 1).

**Table 1. Molecular Characterization of the Synthesized Polymers**

|                       | molar composition <sup>a</sup><br>(%) |        | $M_n^b$ (kDa) | $M_w^b$ (kDa) | $\bar{D}^b$ |
|-----------------------|---------------------------------------|--------|---------------|---------------|-------------|
|                       | <i>t</i> BA (%)                       | UR (%) |               |               |             |
| <i>pt</i> BA(100)     | 100                                   | 0      | 91            | 145           | 1.6         |
| <i>t</i> BA(89)UR(11) | 89                                    | 11     | 98            | 137           | 1.4         |
| <i>t</i> BA(79)UR(21) | 79                                    | 21     | 88            | 168           | 1.9         |
| <i>t</i> BA(68)UR(32) | 68                                    | 32     | 83            | 123           | 1.5         |
| <i>t</i> BA(57)UR(43) | 57                                    | 43     | 92            | 163           | 1.7         |
| <i>t</i> BA(47)UR(53) | 47                                    | 53     | 91            | 117           | 1.3         |

<sup>a</sup>Determined by <sup>1</sup>H NMR spectroscopy in CDCl<sub>3</sub>. <sup>b</sup>Determined by SEC with a refractive index detector and PMMA standards in THF.

The <sup>1</sup>H NMR spectra were obtained prior to TFA treatment to determine the molar compositions of the copolymers (Figures 2b and S3). The spectra of all copolymers exhibit characteristic signals (**e**) at 3.2 ppm, corresponding to the methylene groups (–CH<sub>2</sub>–) of the *n*-butyl carbamate side chains. The signals corresponding to the methine groups (–CH–) of the polyacrylate backbone (**b** and **b'**) are observed at 2.1–2.4 ppm. The molar composition of *t*BA and BCOE in the random copolymer is calculated by comparing the integral ratios of **e** and **b** + **b'** (see Supporting Information for further details), and the calculated compositions of the copolymers and feed ratios are consistent (Table S1). TFA treatment results in the complete disappearance of the signal representing the methyl groups (–CH<sub>3</sub>) of *t*-butyl groups (**i**). Subsequently, a new signal is observed at  $\sim$ 12.4 ppm (**i'**) owing to the generation of the carboxylic acid groups (–COOH).

FT-IR spectroscopy further confirmed the successful deprotection of the copolymer. As shown in Figure 2c, a wide band is observed at 3300–2500 cm<sup>-1</sup> after TFA treatment, which corresponds to the –OH stretching mode of carboxylic acid. In addition, the peak representing the C = O stretching vibration broadens and shifts slightly from 1721 to



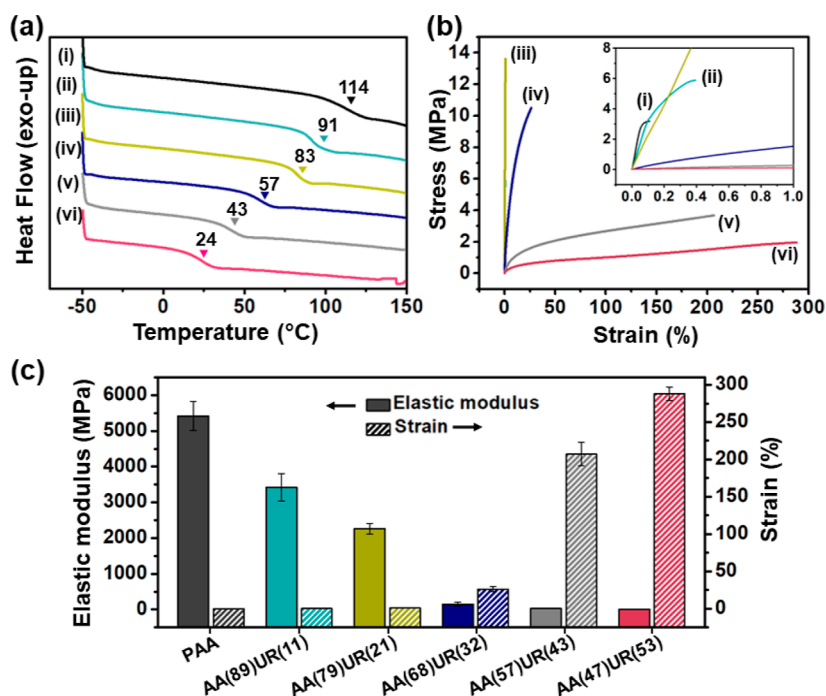


**Figure 3.** Thermal and mechanical properties of PAA and the copolymers: (a,b) DSC thermograms and stress–strain curves of (i) PAA, (ii) AA(89)UR(11), (iii) AA(79)UR(21), (iv) AA(68)UR(32), (v) AA(57)UR(43), and (vi) AA(47)UR(53), and (c) a summary of their mechanical properties.

1702  $\text{cm}^{-1}$ , indicating the generation of carboxylic acid groups within the copolymer. The broadening and slight blue-shifting of the carbonyl stretching band, along with the apparent shoulder peak close to the N–H stretching mode (3085  $\text{cm}^{-1}$ ), confirm the presence of hydrogen bonding within the copolymer. Thus, the results of SEC and  $^1\text{H}$  NMR and FT-IR spectroscopies confirm the successful syntheses of the random copolymers with the desired molecular weights and compositions.

**Thermal and Mechanical Properties.** The thermal properties of the copolymers were initially investigated through DSC, and the second heating curves are shown in Figure 3a. The  $T_g$  values of the copolymers gradually decrease from 114 to 24 °C with a gradual increase in the UR content due to the large free volume created by the bulky *n*-butyl carbamate groups. Notably, the poly(BCOE) homopolymer is much compliant ( $T_g = -3$  °C) compared to PAA.<sup>42</sup> The observed dependence of  $T_g$  on the incorporation of flexible side chains is consistent with previous studies.<sup>44,45</sup> Adjusting the UR content also drastically alters the mechanical properties of the copolymers, as shown in Figure 3b,c, and Table 2. The copolymers with >43 mol % UR content, in particular, may

undergo considerable elongation (>200%), whereas those with UR content of <32 mol % are relatively stiff. According to previous studies, neither an excessively brittle nor a deformable binder is desirable in accommodating the stress generated during the volume change of Si.<sup>22,44,46–48</sup> Thus, copolymers with moderate UR content, such as AA(89)UR(11), AA(79)UR(21), and AA(68)UR(32), are better candidates for use as high-performance binders in Si anodes in terms of mechanical properties.

**Self-Healing.** As poly(BCOE) is known to undergo autonomous self-healing owing to its low  $T_g$  and abundance of hydrogen bonds,<sup>42</sup> the healing property may be also imparted to our copolymers if a sufficient number of UR groups is incorporated. Three representative samples containing low, moderate, and high contents of UR, AA(89)UR(11), AA(68)UR(32), and AA(47)UR(53), respectively, were used to investigate the self-healing characteristics. The film samples (thicknesses  $\approx 150$   $\mu\text{m}$ ) were manually scratched with a razor blade under identical pressures, and then the depths of the scratches were monitored at different time intervals through laser confocal microscopy. As shown in Figure 4a, the AA(68)UR(32) and AA(47)UR(53) specimens exhibit healing after 2 h, whereas the scratch in AA(89)UR(11) remains. As the electrode is wet with the electrolyte during electrochemical characterization, the healing of the binders was also evaluated in the presence of the electrolyte. After the surface was scratched in a similar manner, 10  $\mu\text{L}$  of the electrolyte was dropped onto the scratched surface. The addition of electrolyte effectively reduced the healing time of the AA(68)UR(32) film from 2 to 1 h, perhaps due to the plasticizing effect. However, healing of the AA(89)UR(11) film is still not observed owing to insufficient chain mobility (i.e., the high  $T_g$ ), even after the addition of a drop of electrolyte (Figure 4b).

Furthermore, to quantify the healing efficiency of the AA(68)UR(32) binder, the tensile properties of the healed

**Table 2. Mechanical Properties of the Polymers**

| polymer      | elastic modulus (MPa) <sup>a</sup> | strain (%) <sup>a</sup> | tensile strength (MPa) <sup>a</sup> |
|--------------|------------------------------------|-------------------------|-------------------------------------|
| PAA          | 5415                               | 0.1                     | 3                                   |
| AA(89)UR(11) | 3420                               | 0.4                     | 6                                   |
| AA(79)UR(21) | 2261                               | 1                       | 14                                  |
| AA(68)UR(32) | 150                                | 26                      | 10.5                                |
| AA(57)UR(43) | 26                                 | 207                     | 4                                   |
| AA(47)UR(53) | 7                                  | 288                     | 2                                   |

<sup>a</sup>Determined from stress–strain curves obtained at 25 °C using a tension film clamp.

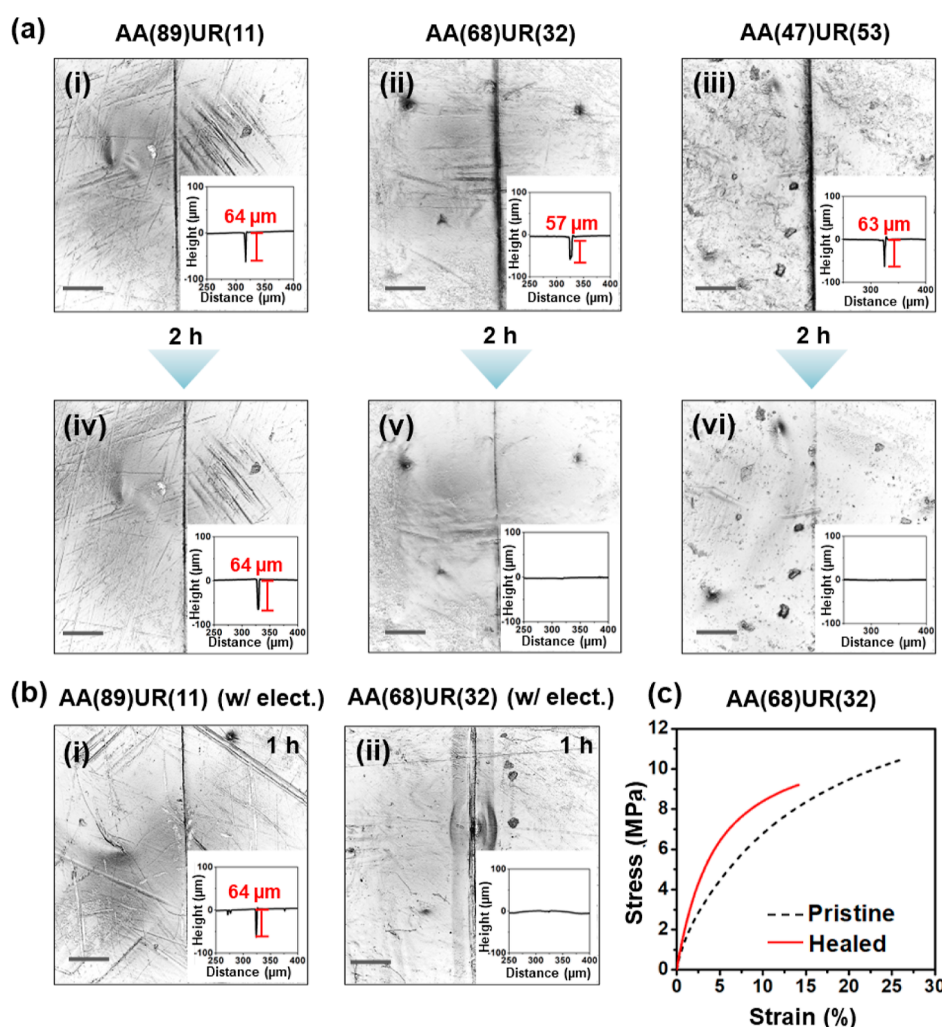


**Figure 4.** Healing tests of various copolymer films [AA(89)UR(11), AA(68)UR(32), and AA(47)UR(53)] in the (a) absence and (b) presence of the electrolyte. Laser confocal microscope images and the corresponding depth profiles (insets) of the scratched surfaces before [a-(i), a-(ii), and a-(iii)] and after healing [a-(iv), a-(v), a-(vi), b-(i), b-(ii), and b-(iii)] at room temperature. The scale bars represent 100  $\mu\text{m}$ . (c) Stress–strain curves of the AA(68)UR(32) film before and after the healing test.

and pristine films were compared. The broken segments of AA(68)UR(32) after the tensile measurement were gently stacked, enabling the boundaries to overlap ( $\sim 1$  mm), followed by the addition of the electrolyte at the overlapped surfaces. Finally, the healed sample was stretched until failure; the corresponding stress–strain curve is shown in Figure 4c. The tensile strength of the healed AA(68)UR(32) film is almost regained with a healing efficiency of 86%. Our results suggest that the healing efficiency is mainly determined by the UR content of the copolymer affecting the segmental mobility as well as by the presence of the electrolyte inducing the plasticizing effects of the solvent molecules.

**Electrochemical Characterization.** The electrochemical properties of the Si electrodes containing 15 wt % of the binders were investigated via galvanostatic cycling studies in a half-cell; the results are shown in Figure 5 and Table S2. An electrolyte solution containing FEC (10%) was used to promote the formation of a stable SEI layer.<sup>49–51</sup> All samples were initially evaluated at an active material loading of  $\sim 0.5$  mg  $\text{cm}^{-2}$ . The initial Coulombic efficiency (ICE) of the Si electrode depends strongly on the molar composition of the binder, and the use of copolymers containing higher UR contents leads to lower ICEs (Figure 5a,b). Generally, a low

ICE is caused by the irreversible loss of Li ions due to parasitic reactions at the electrode/electrolyte interface, leading to the formation of a thick SEI layer. Therefore, the low ICEs of the electrodes containing the copolymers with a high UR content are attributed to the increased consumption of the electrolyte by the corresponding binders. To confirm this, the degrees of swelling of the binders in the electrolyte were investigated (Figure S4). The binders with UR content of  $\geq 43$  mol % absorb considerable amounts of the electrolyte and become sticky, whereas those with UR content of 0–32 mol % display low or moderate degrees of swelling (1.3–14.3%). Notably, the moderate swelling of the binder in the electrolyte (10–20%) is preferred, because it facilitates ion transport within the electrode.<sup>52</sup> Thus, the high electrolyte uptake of the AA(S7)-UR(43) and AA(47)UR(53) binders likely facilitates side reactions at the electrode interfaces and decreases the ICEs.

The specific discharge capacities of the Si electrodes prepared by using the copolymer binders, Si-AA(xx)UR(yy), were initially investigated over 100 cycles (Figure 5c). Interestingly, increasing the UR content of the copolymer from 11 to 32 mol % gradually improves the cycling performance with high initial discharge capacity, thus outperforming Si-PAA. However, further increasing the UR

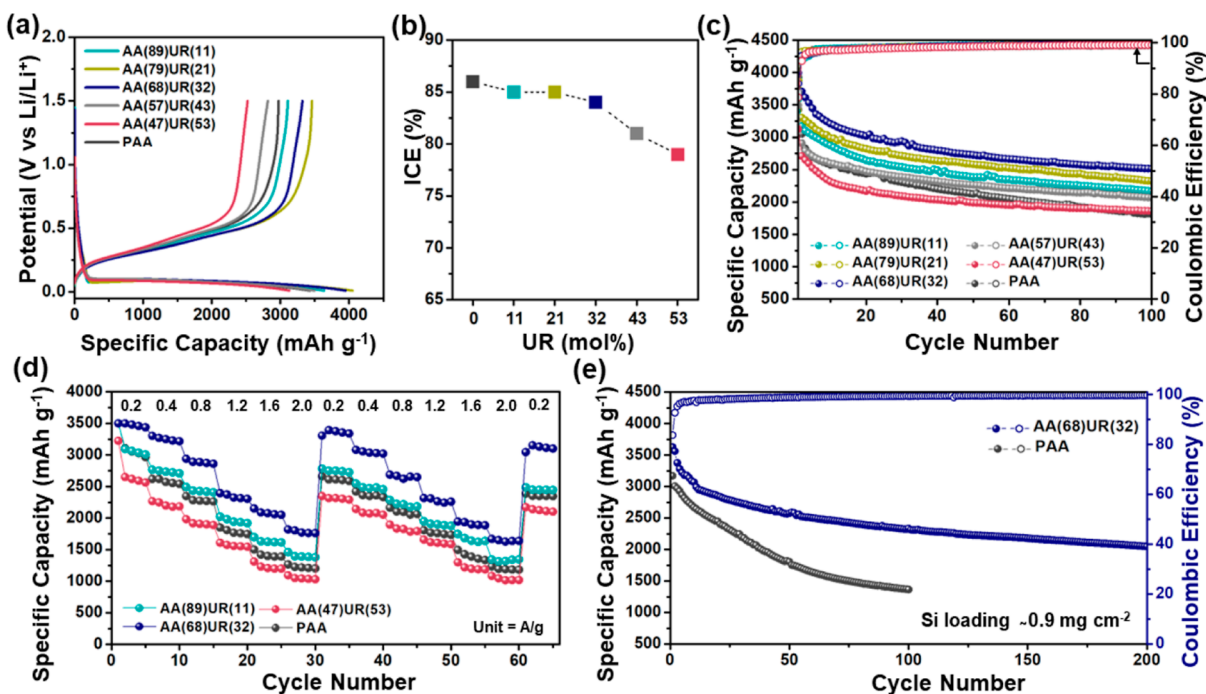


**Figure 5.** Electrochemical properties of the Si electrodes prepared using various copolymer binders. (a) First lithiation and delithiation profiles, (b) ICEs, (c) cycling performance at a current density of  $0.5 \text{ A g}^{-1}$  (Si loading  $\approx 0.5 \text{ mg cm}^{-2}$ ), (d) rate performance with varying the current density from  $0.2$  to  $2.0 \text{ A g}^{-1}$  with a fixed capacity of  $3500 \text{ mA h g}^{-1}$ , and (e) cycling performance of Si-AA(68)UR(32) and Si-PAA with high mass loadings (Si loadings  $\approx 0.9 \text{ mg cm}^{-2}$ ).

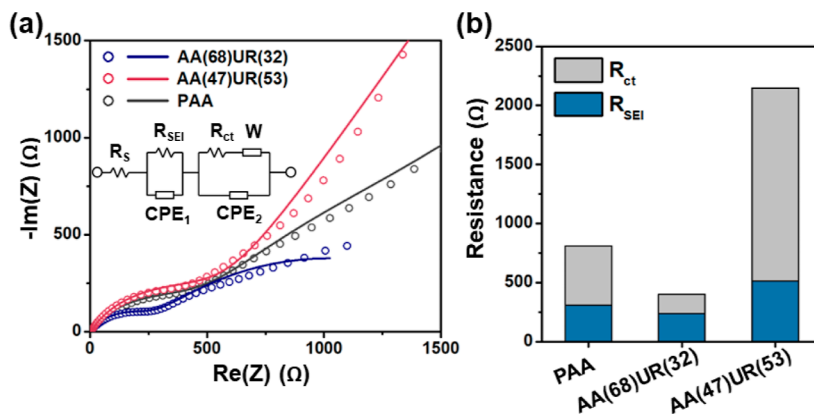


**Figure 6.** (a) Nyquist plots and (b) summary of EIS results of the Si electrodes at their 50th cycles.

content (i.e., 43 or 53 mol %) of the binder decreases the cycling performance. The low specific capacities of Si-AA(57)UR(43) and Si-AA(47)UR(53) may be associated with their low ICEs, which inhibit Li ion transport. The highly compliant natures of these binders are also inadequate in preserving the structural integrity of the electrode.

The rate performance of Si-AA(89)UR(11), Si-AA(68)UR(32), Si-AA(47)UR(53), and Si-PAA was compared by varying the current density from  $0.2$  to  $2.0 \text{ A g}^{-1}$  (Figure 5d). Consistent with the cycling performance at a constant current, Si-AA(68)UR(32) exhibits the highest capacity at all current densities, whereas Si-AA(47)UR(53) displays the lowest capacity. Si-AA(68)UR(32) was still able to deliver  $1640 \text{ mA h g}^{-1}$  at  $2.0 \text{ A g}^{-1}$  after 60 cycles at different current densities. When the current density returns to  $0.2 \text{ A g}^{-1}$ , the capacity of Si-AA(68)UR(32) recovers to  $3045 \text{ mA h g}^{-1}$ , which corresponds to 89% of the original capacity (at the fifth

cycle). The Si-AA(68)UR(32) and Si-PAA cells were further compared at high current densities of  $4.0$  and  $8.0 \text{ A g}^{-1}$ . Notably, the Si-AA(68)UR(32) cell maintained high-capacity levels (Figure S5).

The effect of the binder on the Si anode can be more dramatic at a high mass loading. As Si-AA(68)UR(32) exhibits the optimal cycling and rate performances among other electrodes, we further evaluated its long-term cycling performance at a high mass loading ( $\sim 0.9 \text{ mg cm}^{-2}$ ). As shown in Figure 5e, Si-AA(68)UR(32) delivers  $2051 \text{ mA h g}^{-1}$  after 200 cycles, corresponding to a capacity retention of 64%, whereas the capacity of Si-PAA plummets to  $1367 \text{ mA h g}^{-1}$  after 100 cycles. These results suggest that AA(68)UR(32) is the optimal binder in our copolymer series for use in a Si anode.

To gain insight into the superior performance of Si-AA(68)UR(32), the interfacial resistance after 50 cycles was investigated via EIS. The Nyquist plot and equivalent



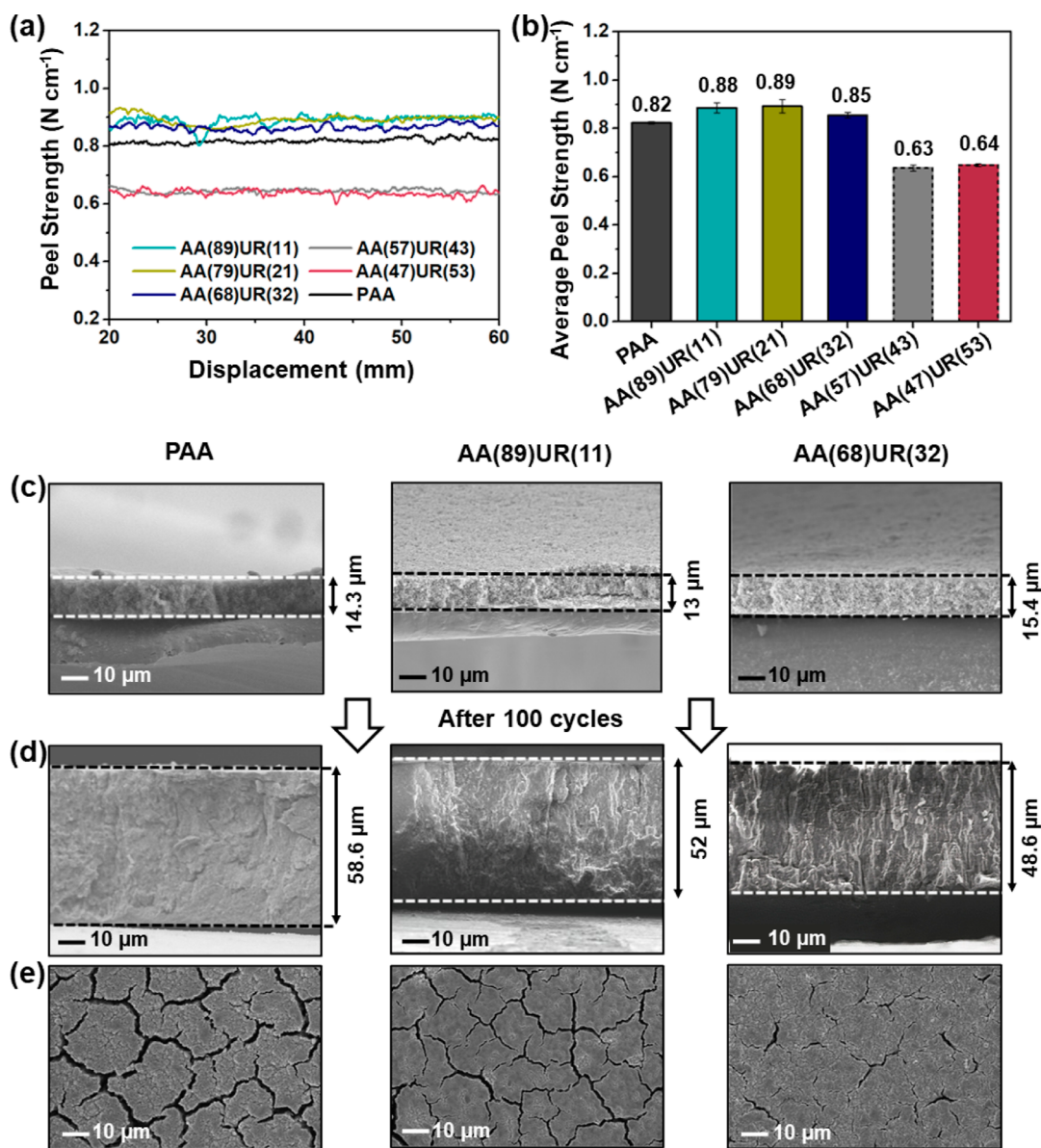


**Figure 7.** (a) Peel strength and (b) average peel strength of the Si electrodes prepared by using various binders. Morphologies of Si-PAA (left), Si-AA(89)UR(11) (middle), and Si-AA(68)UR(32) (right): (c) cross sections before cycling and (d) after 100 cycles and (e) surfaces after 100 cycles.

diagram are shown in Figures 6a and S6, and the corresponding resistances are provided in the Supporting Information (Table S3). All Nyquist plots consist of semi-circles in the high-mid frequency region that represent a combination of the interfacial resistances due to SEI growth ( $R_{SEI}$ ) and charge transfer resistances ( $R_{ct}$ ). The slope at a low frequency represents the Warburg impedance ( $Z_w$ ), which is related to Li ion diffusion at the interface. Based on regression, Si-AA(68)UR(32) exhibits the lowest resistance ( $R_{ct} + R_{SEI} = 399 \Omega$ ) compared to Si-PAA ( $810 \Omega$ ) and Si-AA(47)UR(53) ( $2147 \Omega$ , Figure 6b), and the  $R_{ct}$  of Si-AA(68)UR(32) ( $160 \Omega$ ) is only one-third of that of Si-PAA ( $500 \Omega$ ). Si-AA(68)UR(32) also exhibits the highest Li ion diffusivity ( $D_{Li^+}$ ); these values and calculation details are provided in the Supporting Information (Figure S7 and Table S4). These results suggest that the migration of Li ions and electrons in Si-AA(68)UR(32) is faster than that in other electrodes, resulting in high specific capacity and rate capability. In contrast, Si-

AA(47)UR(53) exhibits a 10-fold higher  $R_{ct}$  and the lowest diffusivity, resulting in the lowest specific capacity.

**Adhesion and Morphologies.** Adhesion is a core function of the binder. To evaluate the adhesion strength of the binders, a 180° peeling study was conducted by using the Si electrodes (Figure 7a,b). Si-AA(79)UR(21) and Si-AA(89)UR(11) display the highest average peel strength ( $0.89$  and  $0.88 \text{ N cm}^{-1}$ , respectively), followed by Si-AA(68)UR(32) ( $0.85 \text{ N cm}^{-1}$ ) and Si-PAA ( $0.82 \text{ N cm}^{-1}$ ). These results suggest that the incorporation of a moderate number of *n*-butyl carbamate groups in the binder does not sacrifice adhesion, but may result in comparable or slightly enhanced adhesion compared to that of Si-PAA. However, further increasing the UR content ( $>32 \text{ mol } \%$ ) decreases the adhesion strength, suggesting that the contribution of the carboxylic acid groups to adhesion is more significant than that of the *n*-butyl carbamate groups. Additionally, the concentration of long, randomly distributed aliphatic side chains in the binders with

high UR content may obstruct the efficient interactions between the carboxylic acid groups and the Si surface.

To determine the correlation between the electrode morphology and electrochemical performance, the thicknesses of the selected electrodes were examined via SEM before cycling and after 100 cycles (Figure 7c,d). While expansion is inevitable for all electrodes, the expansion of Si-AA(68)-UR(32) is considerably smaller (216%) than that of Si-PAA (310%) and Si-AA(89)UR(11) (300%). Remarkably, the surface of Si-AA(68)UR(32) exhibits fewer shallow cracks, whereas increased numbers of larger cracks are observed on the Si-PAA and Si-AA(89)UR(11) surfaces (Figure 7e). Therefore, the superior structural integrity of Si-AA(68)-UR(32) can be retained during electrochemical cycling, emphasizing the significance of using an appropriate binder with the Si electrode. Notably, the healing capability of AA(68)UR(32) is the most distinguishing characteristic compared to those of PAA and AA(89)UR(11), suggesting the significance of the abundant hydrogen bonding interactions of this binder.

In our binder series, the number of carboxylic acid groups is associated with adhesion, whereas that of the *n*-butyl carbamate groups is linked to the self-healing, deformability, and electrolyte uptake of the binder. Additionally, these properties can be effectively tuned and thus optimized by altering the composition of the copolymer binder during synthesis. The radar plot shown in Figure 8 summarizes

structural integrity of the electrode and further enhance the cycling performance.

## CONCLUSIONS

A new series of random copolymers containing various contents of carboxylic acid and *n*-butyl carbamate groups were synthesized and successfully employed as binders in Si electrodes. The structure–property relationship of these copolymers, i.e., thermal, mechanical, self-healing, and adhesion properties, was systematically investigated and correlated with the electrochemical performance of the Si electrodes. Binders with well-balanced properties, such as adequate mechanical properties, strong adhesion, low-to-moderate electrolyte uptake, and self-healing characteristics, were more favorable for the high electrochemical performance of the Si electrode in relation to binders with biased properties. Adhesion strength and mechanical properties, in particular, should be prioritized over self-healing. Overall, this study provides a useful guide for the molecular engineering of binders to address the challenges of Si anodes and potentially other conversion-type anodes.

## ASSOCIATED CONTENT

### Supporting Information

The Supporting Information is available free of charge at <https://pubs.acs.org/doi/10.1021/acsaem.3c02825>.

XRD patterns of SiNP; SEC and  $^1\text{H}$  NMR spectra; calculation method and details of molar composition of copolymers; electrolyte uptake of binder films and photographs of binder films immersed in electrolyte; summary of electrochemical properties of Si electrodes; rate performance of selected samples at high current densities; summary of impedance analysis of Si electrodes after 50 cycles;  $\text{Re}(Z)$  vs  $\omega^{-0.5}$  plots of Si electrodes after 50 cycles; and details of calculation and values of  $\text{Li}^+$  ion diffusivity (PDF)

## AUTHOR INFORMATION

### Corresponding Authors

Il Tae Kim – Department of Chemical and Biological Engineering, Gachon University, Seongnam-si, Gyeonggi-do 13120, Republic of Korea; [orcid.org/0000-0002-8857-0061](https://orcid.org/0000-0002-8857-0061); Email: [itkim@gachon.ac.kr](mailto:itkim@gachon.ac.kr)

Suk-kyun Ahn – School of Chemical Engineering, Pusan National University, Busan 46241, Republic of Korea; [orcid.org/0000-0002-6841-4213](https://orcid.org/0000-0002-6841-4213); Email: [skahn@pusan.ac.kr](mailto:skahn@pusan.ac.kr)

### Authors

Anjali Nagapadi Preman – School of Chemical Engineering, Pusan National University, Busan 46241, Republic of Korea

Thuan Ngoc Vo – Department of Chemical and Biological Engineering, Gachon University, Seongnam-si, Gyeonggi-do 13120, Republic of Korea; [orcid.org/0000-0003-3211-3539](https://orcid.org/0000-0003-3211-3539)

Subi Choi – School of Chemical Engineering, Pusan National University, Busan 46241, Republic of Korea

Hyocheol Lee – School of Chemical Engineering, Pusan National University, Busan 46241, Republic of Korea

Ye Eun Lim – Department of Chemical and Biological Engineering, Gachon University, Seongnam-si, Gyeonggi-do 13120, Republic of Korea

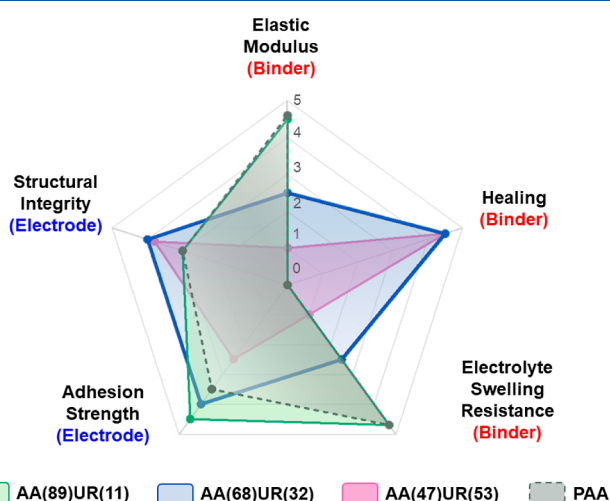


Figure 8. Radar plot of the key properties of the representative copolymers and the PAA binder.

various properties of the representative copolymer and PAA binders. Based on our observations, strong adhesion and adequate mechanical properties (i.e., neither too stiff nor too deformable) are essential in generating high-performance binders, whereas the healing property is not the highest priority. Nevertheless, the self-healing of a binder can be useful in further enhancing the electrochemical performance by stabilizing the electrode morphology as long as good adhesion and mechanical properties are ensured. Among all binders, AA(68)UR(32) exhibits well-balanced properties, such as adequate mechanical properties, strong adhesion, moderate electrolyte uptake, and self-healing, leading to the optimal electrochemical performance when employed in a Si electrode. A 3D cross-linked network of this binder may improve the

Complete contact information is available at:  
<https://pubs.acs.org/10.1021/acsaem.3c02825>

## Author Contributions

The manuscript was written through contributions of all authors. All authors have given approval to the final version of the manuscript.

## Notes

The authors declare no competing financial interest.

## ACKNOWLEDGMENTS

This work was supported by the two-year Research Grant of Pusan National University.

## REFERENCES

- (1) Armand, M.; Tarascon, J. M. Building better batteries. *Nature* **2008**, *451*, 652–657.
- (2) Wu, H.; Cui, Y. Designing nanostructured Si anodes for high energy lithium ion batteries. *Nano Today* **2012**, *7*, 414–429.
- (3) Janek, J.; Zeier, W. G. A solid future for battery development. *Nat. Energy* **2016**, *1*, 16141.
- (4) Munaoka, T.; Yan, X.; Lopez, J.; To, J. W. F.; Park, J.; Tok, J. B.-H.; Cui, Y.; Bao, Z. Ionically Conductive Self-Healing Binder for Low Cost Si Microparticles Anodes in Li-Ion Batteries. *Adv. Energy Mater.* **2018**, *8*, 1703138.
- (5) Li, P.; Zhao, G.; Zheng, X.; Xu, X.; Yao, C.; Sun, W.; Dou, S. X. Recent progress on silicon-based anode materials for practical lithium-ion battery applications. *Energy Storage Mater.* **2018**, *15*, 422–446.
- (6) Kwon, T.-w.; Choi, J. W.; Coskun, A. The emerging era of supramolecular polymeric binders in silicon anodes. *Chem. Soc. Rev.* **2018**, *47*, 2145–2164.
- (7) Chan, C. K.; Ruffo, R.; Hong, S. S.; Huggins, R. A.; Cui, Y. Structural and electrochemical study of the reaction of lithium with silicon nanowires. *J. Power Sources* **2009**, *189*, 34–39.
- (8) Cao, P.-F.; Yang, G.; Li, B.; Zhang, Y.; Zhao, S.; Zhang, S.; Erwin, A.; Zhang, Z.; Sokolov, A. P.; Nanda, J.; Saito, T. Rational Design of a Multifunctional Binder for High-Capacity Silicon-Based Anodes. *ACS Energy Lett.* **2019**, *4*, 1171–1180.
- (9) Teki, R.; Datta, M. K.; Krishnan, R.; Parker, T. C.; Lu, T.-M.; Kumta, P. N.; Koratkar, N. Nanostructured Silicon Anodes for Lithium Ion Rechargeable Batteries. *Small* **2009**, *5*, 2236–2242.
- (10) Cho, J. Porous Si anode materials for lithium rechargeable batteries. *J. Mater. Chem.* **2010**, *20*, 4009–4014.
- (11) Li, X.; Gu, M.; Hu, S.; Kennard, R.; Yan, P.; Chen, X.; Wang, C.; Sailor, M. J.; Zhang, J.-G.; Liu, J. Mesoporous silicon sponge as an anti-pulverization structure for high-performance lithium-ion battery anodes. *Nat. Commun.* **2014**, *5*, 4105.
- (12) Yan, L.; Liu, J.; Wang, Q.; Sun, M.; Jiang, Z.; Liang, C.; Pan, F.; Lin, Z. In Situ Wrapping Si Nanoparticles with 2D Carbon Nanosheets as High-Areal-Capacity Anode for Lithium-Ion Batteries. *ACS Appl. Mater. Interfaces* **2017**, *9*, 38159–38164.
- (13) Jia, D.; Li, X.; Huang, J. Bio-inspired sandwich-structured carbon/silicon/titanium-oxide nanofibers composite as an anode material for lithium-ion batteries. *Composites, Part A* **2017**, *101*, 273–282.
- (14) Preman, A. N.; Lee, H.; Yoo, J.; Kim, I. T.; Saito, T.; Ahn, S.-k. Progress of 3D network binders in silicon anodes for lithium ion batteries. *J. Mater. Chem. A* **2020**, *8*, 25548–25570.
- (15) Eshetu, G. G.; Figgemeier, E. Confronting the Challenges of Next-Generation Silicon Anode-Based Lithium-Ion Batteries: Role of Designer Electrolyte Additives and Polymeric Binders. *ChemSusChem* **2019**, *12*, 2515–2539.
- (16) Burdette-Trofimov, M. K.; Armstrong, B. L.; Rogers, A. M.; Heroux, L.; Doucet, M.; Yang, G.; Phillip, N. D.; Kidder, M. K.; Veith, G. M. Understanding Binder-Silicon Interactions during Slurry Processing. *J. Phys. Chem. C* **2020**, *124*, 13479–13494.
- (17) Deng, L.; Zheng, Y.; Zheng, X.; Or, T.; Ma, Q.; Qian, L.; Deng, Y.; Yu, A.; Li, J.; Chen, Z. Design Criteria for Silicon-Based Anode Binders in Half and Full Cells. *Adv. Energy Mater.* **2022**, *12*, 2200850.
- (18) Li, J.; Lewis, R. B.; Dahn, J. R. Sodium Carboxymethyl Cellulose. *Electrochem. Solid-State Lett.* **2007**, *10*, A17.
- (19) Wei, L.; Chen, C.; Hou, Z.; Wei, H. Poly (acrylic acid sodium) grafted carboxymethyl cellulose as a high performance polymer binder for silicon anode in lithium ion batteries. *Sci. Rep.* **2016**, *6*, 19583.
- (20) Kovalenko, I.; Zdyrko, B.; Magasinski, A.; Hertzberg, B.; Milicev, Z.; Burtovyy, R.; Luzinov, I.; Yushin, G. A Major Constituent of Brown Algae for Use in High-Capacity Li-Ion Batteries. *Science* **2011**, *334*, 75–79.
- (21) Magasinski, A.; Zdyrko, B.; Kovalenko, I.; Hertzberg, B.; Burtovyy, R.; Huebner, C. F.; Fuller, T. F.; Luzinov, I.; Yushin, G. Toward efficient binders for Li-ion battery Si-based anodes: polyacrylic acid. *ACS Appl. Mater. Interfaces* **2010**, *2*, 3004–3010.
- (22) Pan, Y.; Ge, S.; Rashid, Z.; Gao, S.; Erwin, A.; Tsukruk, V.; Vogiatzis, K. D.; Sokolov, A. P.; Yang, H.; Cao, P.-F. Adhesive Polymers as Efficient Binders for High-Capacity Silicon Electrodes. *ACS Appl. Energy Mater.* **2020**, *3*, 3387–3396.
- (23) Xu, Z.; Yang, J.; Zhang, T.; Nuli, Y.; Wang, J.; Hirano, S.-i. Silicon Microparticle Anodes with Self-Healing Multiple Network Binder. *Joule* **2018**, *2*, 950–961.
- (24) Zhang, S.; Liu, K.; Xie, J.; Xu, X.; Tu, J.; Chen, W.; Chen, F.; Zhu, T.; Zhao, X. An Elastic Cross-Linked Binder for Silicon Anodes in Lithium-Ion Batteries with a High Mass Loading. *ACS Appl. Mater. Interfaces* **2023**, *15*, 6594–6602.
- (25) Wan, X.; Kang, C.; Mu, T.; Zhu, J.; Zuo, P.; Du, C.; Yin, G. A Multilevel Buffered Binder Network for High-Performance Silicon Anodes. *ACS Energy Lett.* **2022**, *7*, 3572–3580.
- (26) Koo, B.; Kim, H.; Cho, Y.; Lee, K. T.; Choi, N.-S.; Cho, J. A Highly Cross-Linked Polymeric Binder for High-Performance Silicon Negative Electrodes in Lithium Ion Batteries. *Angew. Chem., Int. Ed.* **2012**, *51*, 8762–8767.
- (27) Choi, S.; Kwon, T.-w.; Coskun, A.; Choi, J. W. Highly elastic binders integrating polyrotaxanes for silicon microparticle anodes in lithium ion batteries. *Science* **2017**, *357*, 279–283.
- (28) Jiao, X.; Yin, J.; Xu, X.; Wang, J.; Liu, Y.; Xiong, S.; Zhang, Q.; Song, J. Highly Energy-Dissipative, Fast Self-Healing Binder for Stable Si Anode in Lithium-Ion Batteries. *Adv. Funct. Mater.* **2021**, *31*, 2005699.
- (29) Wang, Y.; Xu, H.; Chen, X.; Jin, H.; Wang, J. Novel constructive self-healing binder for silicon anodes with high mass loading in lithium-ion batteries. *Energy Storage Mater.* **2021**, *38*, 121–129.
- (30) Jeong, Y. K.; Choi, J. W. Mussel-Inspired Self-Healing Metallopolymers for Silicon Nanoparticle Anodes. *ACS Nano* **2019**, *13*, 8364–8373.
- (31) Chen, H.; Wu, Z.; Su, Z.; Chen, S.; Yan, C.; Al-Mamun, M.; Tang, Y.; Zhang, S. A mechanically robust self-healing binder for silicon anode in lithium ion batteries. *Nano Energy* **2021**, *81*, 105654.
- (32) Kwon, T. W.; Jeong, Y. K.; Lee, I.; Kim, T. S.; Choi, J. W.; Coskun, A. Systematic molecular-level design of binders incorporating Meldrum's acid for silicon anodes in lithium rechargeable batteries. *Adv. Mater.* **2014**, *26*, 7979–7985.
- (33) Ryu, J.; Kim, S.; Kim, J.; Park, S.; Lee, S.; Yoo, S.; Kim, J.; Choi, N.-S.; Ryu, J.-H.; Park, S. Room-Temperature Crosslinkable Natural Polymer Binder for High-Rate and Stable Silicon Anodes. *Adv. Funct. Mater.* **2020**, *30*, 1908433.
- (34) Wang, C.; Wu, H.; Chen, Z.; McDowell, M. T.; Cui, Y.; Bao, Z. Self-healing chemistry enables the stable operation of silicon microparticle anodes for high-energy lithium-ion batteries. *Nat. Chem.* **2013**, *5*, 1042–1048.
- (35) Zhang, G.; Yang, Y.; Chen, Y.; Huang, J.; Zhang, T.; Zeng, H.; Wang, C.; Liu, G.; Deng, Y. A Quadruple-Hydrogen-Bonded Supramolecular Binder for High-Performance Silicon Anodes in Lithium-Ion Batteries. *Small* **2018**, *14*, 1801189.
- (36) Malik, Y. T.; Shin, S.-Y.; Jang, J. I.; Kim, H. M.; Cho, S.; Do, Y. R.; Jeon, J.-W. Self-Repairable Silicon Anodes Using a Multifunctional



Binder for High-Performance Lithium-Ion Batteries. *Small* **2023**, *19*, 2206141.

(37) Ryou, M.-H.; Kim, J.; Lee, I.; Kim, S.; Jeong, Y. K.; Hong, S.; Ryu, J. H.; Kim, T.-S.; Park, J.-K.; Lee, H.; Choi, J. W. Mussel-Inspired Adhesive Binders for High-Performance Silicon Nanoparticle Anodes in Lithium-Ion Batteries. *Adv. Mater.* **2013**, *25*, 1571–1576.

(38) Jeong, Y. K.; Kwon, T.-w.; Lee, I.; Kim, T.-S.; Coskun, A.; Choi, J. W. Millipede-inspired structural design principle for high performance polysaccharide binders in silicon anodes. *Energy Environ. Sci.* **2015**, *8*, 1224–1230.

(39) Guo, R.; Zhang, S.; Ying, H.; Yang, W.; Wang, J.; Han, W. Q. New, Effective, and Low-Cost Dual-Functional Binder for Porous Silicon Anodes in Lithium-Ion Batteries. *ACS Appl. Mater. Interfaces* **2019**, *11*, 14051–14058.

(40) Wang, X.; Liu, S.; Zhang, Y.; Wang, H.; Aboalhassan, A. A.; Li, G.; Xu, G.; Xue, C.; Yu, J.; Yan, J.; Ding, B. Highly Elastic Block Copolymer Binders for Silicon Anodes in Lithium-Ion Batteries. *ACS Appl. Mater. Interfaces* **2020**, *12*, 38132–38139.

(41) Yang, J.; Zhang, L.; Zhang, T.; Wang, X.; Gao, Y.; Fang, Q. Self-healing strategy for Si nanoparticles towards practical application as anode materials for Li-ion batteries. *Electrochem. Commun.* **2018**, *87*, 22–26.

(42) Zhang, Z.; Ghezawi, N.; Li, B.; Ge, S.; Zhao, S.; Saito, T.; Hun, D.; Cao, P.-F. Autonomous Self-Healing Elastomers with Unprecedented Adhesion Force. *Adv. Funct. Mater.* **2021**, *31*, 2006298.

(43) Sun, F.; Li, Z.; Gao, S.; He, Y.; Luo, J.; Zhao, X.; Yang, D.; Gao, T.; Yang, H.; Cao, P.-F. Self-Healable, Highly Stretchable, Ionic Conducting Polymers as Efficient Protecting Layers for Stable Lithium-Metal Electrodes. *ACS Appl. Mater. Interfaces* **2022**, *14*, 26014–26023.

(44) Son, J.; Vo, T. N.; Cho, S.; Preman, A. N.; Kim, I. T.; Ahn, S.-k. Acrylic random copolymer and network binders for silicon anodes in lithium-ion batteries. *J. Power Sources* **2020**, *458*, 228054.

(45) Jiang, S.; Hu, B.; Shi, Z.; Chen, W.; Zhang, Z.; Zhang, L. Re-Engineering Poly(Acrylic Acid) Binder toward Optimized Electrochemical Performance for Silicon Lithium-Ion Batteries: Branching Architecture Leads to Balanced Properties of Polymeric Binders. *Adv. Funct. Mater.* **2019**, *30*, 1908558.

(46) Lee, H.; Preman, A. N.; Vo, T. N.; Lee, J.-H.; Kim, I. T.; Ahn, S.-k. In situ crosslinkable acrylic random copolymer binders for silicon anodes in lithium-ion batteries. *Int. J. Energy Res.* **2022**, *46*, 12565–12578.

(47) Li, X.; Chen, H.; Chen, M.; Qi, J.; Chen, S.; Zhuo, H. Ionic Liquid-Decorated Copolymer Binders for Silicon/Graphite Anodes with Enhanced Rate Capability and Excellent Cycle Stability. *ACS Appl. Energy Mater.* **2021**, *4*, 12709–12717.

(48) Chen, C.; Lee, S. H.; Cho, M.; Kim, J.; Lee, Y. Cross-Linked Chitosan as an Efficient Binder for Si Anode of Li-ion Batteries. *ACS Appl. Mater. Interfaces* **2016**, *8*, 2658–2665.

(49) Preman, A. N.; Lim, Y. E.; Lee, S.; Kim, S.; Kim, I. T.; Ahn, S.-k. Facile synthesis of polynorbornene-based binder through ROMP for silicon anode in lithium-ion batteries. *Korean J. Chem. Eng.* **2023**, *40*, 2529–2537.

(50) Xu, C.; Lindgren, F.; Philippe, B.; Gorgoi, M.; Björefors, F.; Edström, K.; Gustafsson, T. Improved Performance of the Silicon Anode for Li-Ion Batteries: Understanding the Surface Modification Mechanism of Fluoroethylene Carbonate as an Effective Electrolyte Additive. *Chem. Mater.* **2015**, *27*, 2591–2599.

(51) Hou, T.; Yang, G.; Rajput, N. N.; Self, J.; Park, S.-W.; Nanda, J.; Persson, K. A. The influence of FEC on the solvation structure and reduction reaction of LiPF<sub>6</sub>/EC electrolytes and its implication for solid electrolyte interphase formation. *Nano Energy* **2019**, *64*, 103881.

(52) Entwistle, J.; Ge, R.; Pardikar, K.; Smith, R.; Cumming, D. Carbon binder domain networks and electrical conductivity in lithium-ion battery electrodes: A critical review. *Renewable Sustainable Energy Rev.* **2022**, *166*, 112624.

The advertisement features a vertical image on the left showing a blue, translucent, spherical object with a yellow, string-like structure emerging from its base, which is surrounded by a cluster of green and pink spheres. The background is a dark blue gradient. Text is overlaid on the right side in white and yellow.

CAS BIOFINDER DISCOVERY PLATFORM™

**PRECISION DATA  
FOR FASTER  
DRUG  
DISCOVERY**

CAS BioFinder helps you identify  
targets, biomarkers, and pathways

**Unlock insights**

**CAS**  
A division of the  
American Chemical Society